frontiers | Frontiers in Earth Science

TYPE Original Research
PUBLISHED 16 January 2023
DOI 10.3389/feart.2022.931611

OPEN ACCESS

EDITED BY
Bjarne Sven Gustav Almqvist,
Uppsala University, Sweden

REVIEWED BY
Xinpeng Pan,
Central South University, China
Jing Ba,
Hohai University, China

*CORRESPONDENCE
Luanxiao Zhao,
zhaoluanxiao@tongji.edu.cn

SPECIALTY SECTION
This article was submitted to Solid Earth Geophysics, a section of the journal Frontiers in Earth Science

RECEIVED 29 April 2022
ACCEPTED 27 October 2022
PUBLISHED 16 January 2023

CITATION
Ali Hussein AA, Zhao L, Chen Y and Wang J (2023), Rock physics characteristics of marine sediments in the South China sea: The link between the geological factors and elastic properties.
Front. Earth Sci. 10:931611.
doi: 10.3389/feart.2022.931611

Rock physics characteristics of marine sediments in the South China sea: The link between the geological factors and elastic properties

Abdullah Ali Ali Hussein[1], Luanxiao Zhao[1]*, Yuanyuan Chen[1] and Jiliang Wang[2]

[1]State Key Laboratory of Marine Geology, Tongji University, Shanghai, China, [2]Institute of Deep-sea Science and Engineering, Chinese Academy of Sciences, Sanya, China

Understanding the geological factors behind the physical and elastic properties of marine sediments and unconsolidated rock is essential for the interpretation of geophysical measurements, hazard assessment, and ocean engineering applications. Core and well logging data from the six drilling sites of the Ocean Drilling Program/International Ocean Discovery Program (ODP/IODP) were used to analyze the rock physical characteristics in the South China sea. The depositional environment plays a significant role in affecting the physical properties of marine sediments. The sediments deposited under shallow water conditions show a higher velocity than the basin, slope, and deeper shelf carbonate deposits. Moreover, the non-depositional hiatus along the Oligocene-Miocene boundary displays a notable control on the variation of rock physical properties. It is found that the lithofacies and physical compaction remarkably influence the elastic characteristics of P-impedance and Vp/Vs ratio. The calcareous-rich sediment and ooze have very low P-impedance and high Vp/Vs ratio, whereas the siltstone and coarse sand present high P-impedance and low Vp/Vs ratio characteristics. With the enhancement of the consolidation degree, the Vp/Vs ratio significantly decreases from 6 to less than 2, suggesting that the shear wave velocity is highly sensitive to physical compactions. The basalt at site U1431 is considerably lower in its P-wave velocity than that at the site of U1433, which is probably caused by the intense fracturing occurring at the site of U1431 associated with different tectonic environments. We establish the link between geological factors and elastic characteristics of marine sediments of SCS, laying the foundation for characterizing depositional environments, lithofacies, and compaction degrees using geophysical measurements.

KEYWORDS

South China sea, rock physics, depositional environment, elastic properties, lithofacies

Introduction

Many geological factors, including lithological variations, compaction conditions, depositional environment, mechanical, and chemical diagenesis, and tectonic activities, can exert notable influence on the elastic characteristics of marine sediments (Ymd, 1973; Hamilton, 1974, 1976, 1980; Hamilton et al., 1982; Richardson et al., 1997; Breitzke, 2000; Eberli et al., 2003; Stewart et al., 2003; Fabricius, 2007, 2014; Ba et al., 2017; Zhang et al., 2020; Zhao et al., 2020; Lyu et al., 2021; Zhang et al., 2021). As a consequence, understanding the rock physical characteristics (especially the elastic signatures) of the marine sediments and unconsolidated rocks plays a critical role in linking geology to geophysical measurements (sonic and surface seismic data). In addition, it also provides important insights into economic resource development, hazard assessment, and ocean engineering applications (Cai et al., 2015; Hughes et al., 2015; Martin et al., 2015; Hou et al., 2018; Graw et al., 2020; Gatter et al., 2021; Ayoub et al., 2022). The primary objective of this study is to systematically analyze the rock physical characteristics in the SCS and their influencing factors based on the ODP/IODPdata.

Using the IODP core and logging data, many researchers have made efforts to understand how the geological factors influence the physical properties of different rocks (e.g., velocity, density, porosity, and attenuation) (Hamilton, 1972; Van der Lingen and Packham, 1975; Nobes et al., 1991; Bassinot et al., 1993; Urmos, 1994; David et al., 1999; Kenter et al., 2002; Kim and Kim, 2005; Courville et al., 2007; Pola et al., 2012; Christeson et al., 2018; Xie et al., 2018; Lee et al., 2021). According to Nobes et al. (1991), the diagenesis, carbonate content, tectonism, lithology, and depositional hiatuses significantly affected the physical rock properties of marine sediments at leg 114 in the South Atlantic. They also point out that the carbonate content and diagenesis decrease porosity and hence increase velocity. Christeson et al. (2018) observed significant variability in velocity, density, and porosity measurements at Hole M0077A due to lithological composition, rate of deposition, shock intensity, and nature of deformation (i.e., density, connectivity, and secondary filling of fractures). Similarly, Van der Lingen and Packham (1975) use DSDP Sites 288 and 289 to evaluate the physical properties of marine sediments, and they found that the differences in physical properties (especially in the porosity) were indicative of differences in diagenesis degree. Furthermore, the results of Kenter et al. (2002) and Eberli et al. (2003) from ODP site 1003 and leg 166, respectively, indicated that porosity, especially the heterogeneous pore structure significantly affects the elastic responses of the carbonate rocks.

It is worth mentioning that the rock physical characteristics of marine sediments and unconsolidated rocks in the SCS are sparsely reported. The SCS has experienced a rapid and narrow transition from the continental breakup with basalt-type magmatism to igneous oceanic crust (Larsen et al., 2018). Based on the results of the ODP/IODP drilling in the SCS, the geological features display a radical contrast reflecting a shift of the depositional facies from terrestrial to shallow and then deep marine (Jian et al., 2019). New drilling results from IODP expeditions 349 and 367/368 represent a change in the depositional environment from the Eocene's coastal-shallow shelf to the Oligocene's outer shelf-slope settings, where the controlling factors might be the nutrient supply and water temperature (Ma et al., 2019). The unique tectonic and depositional environment of the South China Sea may significantly control the physical properties of marine sediments. Moreover, the SCS is a typical deep-water basin, exhibiting high pressure and temperature characteristics. Therefore, the rock physical characteristics in SCS might be different from that of other well-studied marginal seas (e.g., Gulf of Mexico, North Sea), hence affecting its corresponding elastic signatures (Wang et al., 2021).

Therefore, the primary contribution of this study is to systematically analyze the rock physical characteristics in the SCS based on the analysis of the ODP/IODP core and logging data at different sites (U1148, U1431, U1433, U1499, U1501, and U1505). Additionally, we explore the different influences of geological factors such as depositional environment, non-depositional hiatus, lithofacies, physical compaction, and tectonic activity on the physical properties of rocks. We compare and evaluate the rock physical characteristics of different sites in the SCS.

The paper is organized as follows: First, we briefly introduced the geological setting and IODP data of the SCS. Then, we presented a detailed analysis of geological factors' influence on the rock physical properties, especially the elastic signature of P-wave impedance and Vp/Vs ratio. Subsequently, we explored the effects of the carbonate content on the rock physics characteristics and discussed the implications for seismic stratigraphy interpretation.

Geological setting and data description

The South China Sea is considered one of the vast marginal seas in East Asia. As shown in Figure 1, the SCS's deep-sea basin can be further subdivided into three sub-basins, namely the Southwest Sub-basin (SWSB), Northwest Sub-basin (NWSB), and East Sub-basin (ESB). These sub-basins are bounded by the Zhongnan Fault (Figure 1) (Li et al., 2014). The average depth of the SCS oceanic basin is about 4700 m. It is characterized by a complex depositional system that serves as a final basin of sediment particles transported by different currents (Zhou et al., 2019).

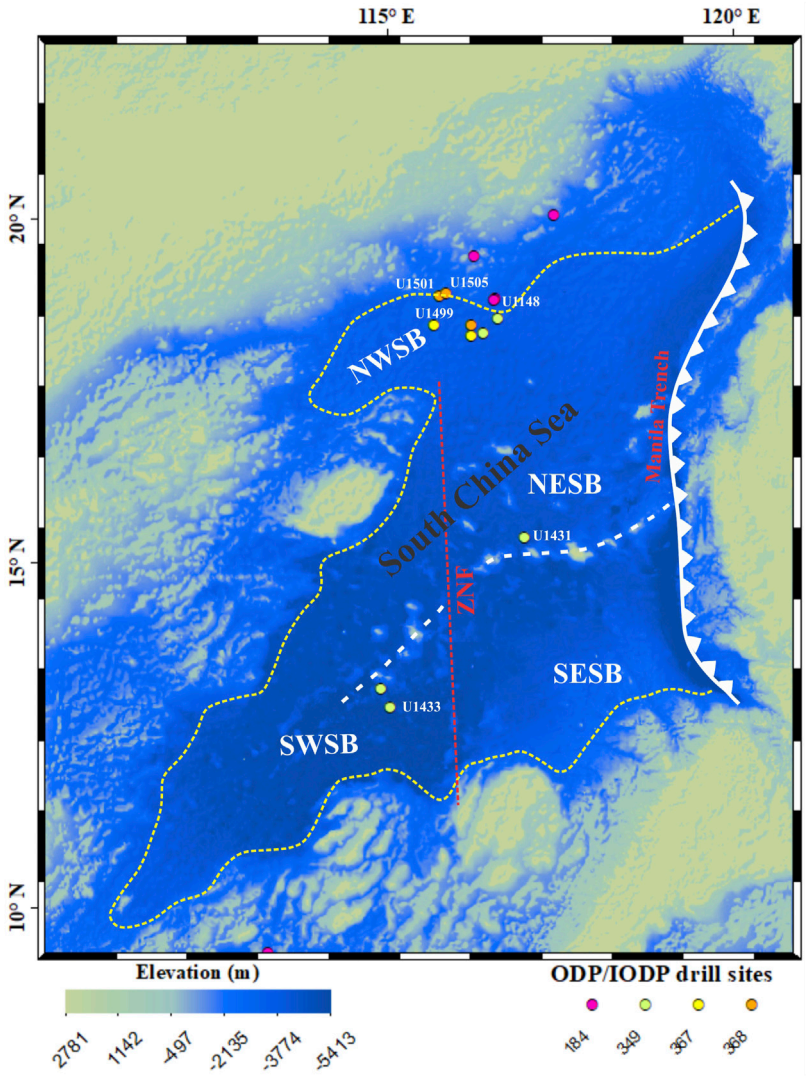

FIGURE 1
Bathymetric map of the (SCS) area. The solid yellow line indicates the ocean continent boundary whereas the red dashed line indicates the Zhongnan Fault (ZNF). The white dashed line shows the fossil-spreading ridge, while white solid line represent the subduction along the Nansha Trough and the Manila Trench. The circles indicate the location of ODP/IODP sites used in this study. SWSB is an abbreviation of the Southwest Sub-basin, NESB, Northeast Sub-basin; SESB, So utheast Sub-basin; NWSB, Northwest Sub-basin.

As displayed in Figure 2, four lithostratigraphic units (I, II, III, and IV) were identified according to the analysis of physical properties and depositional environments by the comparison among the six drilling sites (U1148, U1431, U1433, U1499, U1501, and U1505) in the study area. These units predominantly consist of different lithologies including claystone and clay with common silt, carbonate turbidites, and siliciclastic sediments with the rare existence of thin layers of volcanoclastic breccia in some areas. The early Miocene's lower unit (lithostratigraphic Unit IV) consists mainly of basaltic igneous rocks and a very small amount of clay-rich thin-bedded rocks. A brief description of the four lithostratigraphic units is given as follows:

1) Unit I of the early Miocene to Pleistocene age was deposited in the deep-water environment and dominated by nannofossil carbonate ooze with clay/claystone and negligible silt in some areas. This unit has a relatively high biogenic carbonate content.

2) Unit II includes late Eocene to late Oligocene siliciclastic deposits (Figure 2). The lower part of this unit

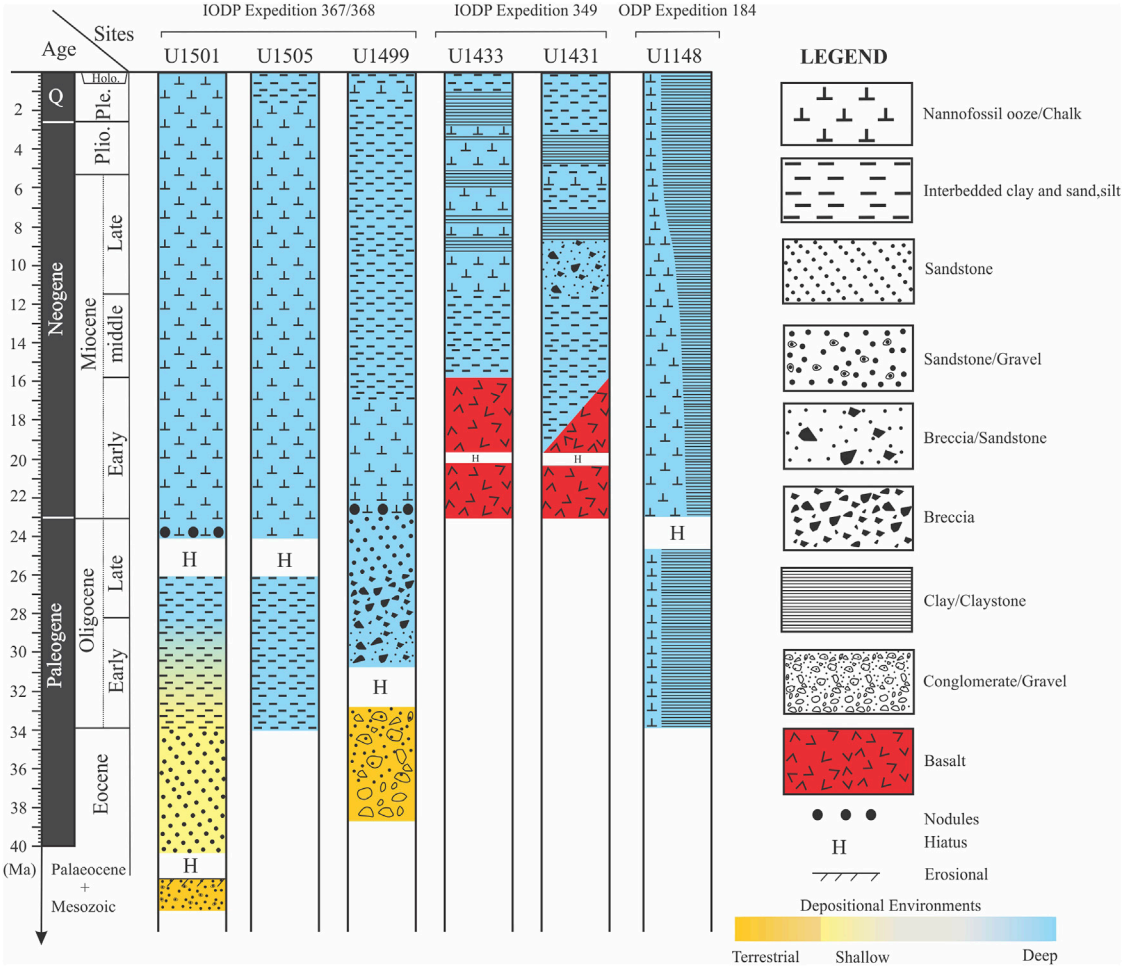

FIGURE 2
A summary of the stratigraphic columns based on deep-sea drilling results from the ODP/IODP South China Sea Sites.

encompasses intervals of coarse sand dominated by shallow water interbedded with dark grey clayey silt containing organic matter. However, the upper part generally reveals a fining upward of clastic material reflecting deep basin situations from the bottom (shallow marine) to the top (bathyal depths). Compared to Unit I, this unit consists of low carbonate content (Figures 3A,B). In contrast, Unit II of the late Miocene to early Pleistocene age at IODP Sites U1431 and U1433 is composed mainly of clay and carbonate ooze interpreted as turbidite deposition, and volcanoclastic breccia interbedded with sandstone, respectively (Li et al., 2015b) indicating high-energy environments. The distinctive layer of volcaniclastic breccia is mainly formed due to several eruptions of volcanic activities from the adjacent seamount (Yan et al., 2014), whereas the source of carbonate turbidite is likely from Dangerous Grounds or Reed Bank (Hutchison and Vijayan, 2010; Franke et al., 2011; Yao et al., 2012; Ding et al., 2013). This suggests rapid redeposition from shallower water settings to a deep-water basin by turbidity currents (Li et al., 2015b).

3) Unit III, of possibly Eocene age, mainly contains coarse sand intervals with clasts up to the size of pebbles at both IODP Sites U1501and U1499. As illustrated in Figure 3B, the sandstone differs from Unit II to Unit III in terms of its physical characteristics, color, degree of lithification, and composition of clastic components. Therefore, Unit III was considered to be established in a littoral-terrestrial environment.
4) Unit IV of the early Miocene is mainly composed of massive basalt lava flows separated by a layer of claystone up to 5 m thick, which clearly shows a variation in the physical properties of the rocks.

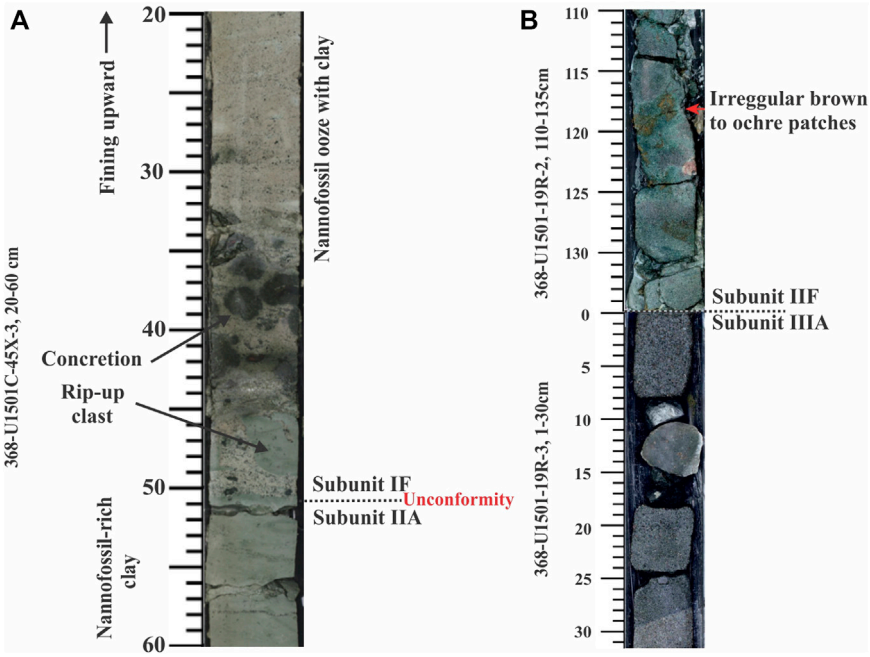

FIGURE 3
(A) Core photo showing the boundary between Units I and II (368-U1501C-45X-3, 20–60 cm) which represent unconformity. Nannofossil ooze with clay and dominates Subunit IF with centimeter-sized concretions at the lower boundary and rip-up clasts. Subunit IIA is dominated by nannofossil-rich clay; **(B)** Images of core section from IODP site U1501 showing the change of lithology from Subunit IIF to Subunit IIIA and the boundary represent non-depositional hiatus. The lower red arrow of Subunit IIF shows irregular brown to ochre and purple patches inferred to be related to diagenetic alteration (Sun et al., 2018).

The data used in this study include cores and well-logging data. Figure 1 shows the sampling locations, and the available data are listed in Table 1. Four sites (U1148, U1499, U1505, and U1501) were drilled in the continental slope and abyssal basin during ODP/IODP Expeditions 184, 367, and 368. They comprise the Cenozoic sediments overlying the basement, and two sites (U1431 and U1433) were drilled in the central basin during IODP Expedition 349 (Table 1). The depth of sites varied between 0 and 1072.15 m from the Eocene to the Pleistocene. The collected data from the expeditions were used to interpret and analyze the rock physical properties such as density, P-wave velocity, and porosity.

Rock physics characteristics and analysis of influencing factors

Influences of depositional units

Figures 4, 5 show the density, velocity, and porosity characteristics of the cored interval of ODP/IODP sites (U1148, U1431, U1433, U1501, and U1505). It is evident that the porosity tends to be inversely related to velocity, whereas density tends to be positively related to velocity.

It can be noted that the different depositional units show distinct rock physical attributes. In unit I, there is a clear increasing trend with depth in density from 1.3 to 1.9 g/cc, P-wave velocity from 1450 to 1930 m/s, and P-impedance from 2000 to 3500 m/s*g/cc. However, the porosity decreases with depth from 79% to 46% (Figures 4A–C). This is most likely due to the loss of organic matter as a result of the water shallowing. It is also associated with an abrupt increase in carbonate content (30 wt%–65 wt%), as nannofossil ooze replaces clay over this interval.

The transitions from unit I to unit II at ODP/IODP sites U1148, U1501, and U1505 show a notable reduction in bulk densities, velocities, and P-impedance as well as an obvious increase in porosities at the Miocene/Oligocene boundary (Figures 4A–C). This change in physical properties showed that the northern SCS was affected by various provenances across the Oligocene/Miocene boundary with non-depositional hiatus possibly formed. At this boundary, the hiatus may have been caused by the effect of a rising sea level, a low supply of terrigenous materials, and comparatively stronger currents in the course of the provenance change (Li et al., 2011). The carbonate-to-clay ratio alters significantly across this boundary. Moreover, more calcareous microfossils are present in Unit 1 than those in Unit II, thus indicating a progressive change of depositional

TABLE 1 Summary of rock physics data used in this study from ODP/IODP Sites in the South China sea.

Expedition	Sites	Depth (m)	Core data					Well log data			
			Porosity	Density	Velocity	Ai	CaCO3	Vp	Vs	Density	Porosity
IODP368	U1501	643.19	✓	✓	✓	✓	✓	✗	✗	✗	✗
	U1505	479.87	✓	✓	✓	✓	✓	✓	✓	✓	✗
IODP 367	U1499	1072.15	✓	✓	✓	✓	✓	✓	✓	✓	✓
IODP 349	U1433	856.69	✓	✓	✓	✓	✓	✓	✓	✓	✗
	U1431	1006.67	✓	✓	✓	✓	✓	✗	✗	✗	✗
ODP 184	1148	844.49	✓	✓	✓	✓	✓	✓	✗	✓	✓

environments from shallow water to deep (lower slope). Such a change is attributed to a reduction in carbonate content from 65% to 10%.

It is necessary to point out that unit II at IODP Site U1501, which comprises siliciclastic sediments, shows some variation in physicalcharacteristics. This is linked to the chaotic depositional environment as well, with the intervening coarse sand to the overall fining of clastic material. The lower part of Unit II between 440 and 600 m comprises coarse sand intervals indicating shallow marine depositional environments with up to pebble-sized clasts, the P-wave velocity, density, and P-impedance can be significantly high, and the porosity can be as low as 8%. It is also interesting to note that the change in depositional environment from shallow water to brackish facies between 510 and 550 m, is associated with a change of lithology from calcareous sandstones to dark grey clayey silt containing organic matter. As we can see in Figure 4B, it shows a higher P-impedance, density, and P-wave velocity than those in the other parts of unit II. The upper part of Unit II between 440 and 380 m shows the overall fining of clastic material indicating shallow water with carbonate content >10%, displaying an increasein density, P-wave velocities, and an abrupt reduction in porosity (from 60% to 35%). In contrast, the major variation in physical properties (increase in P-wave velocity, density, and a decrease in porosity) within Unit II at IODP Sites U1431 and U1433, reflects the massive carbonate and thick breccia interbedded with sandstone (Figures 5A,B), respectively. The transitions from Unit II to Unit III at IODP Sites U1499 and U1501are characterized by a sudden variation in physical properties. An increase in P-wave velocity from 1844–4500 m/s, bulk density

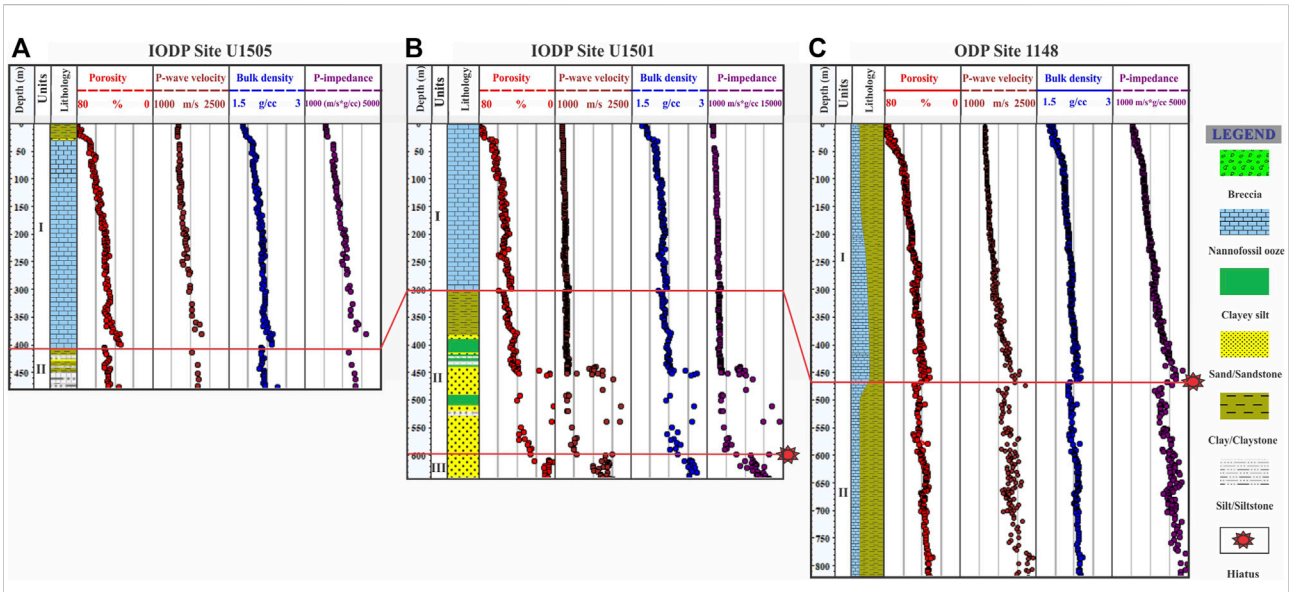

FIGURE 4
Core data results of the studied sites U1501, U1505, and U1148 and the position of non-depositional hiatus, with measurements of moisture, density (MAD), P-wave velocity (PWC), and P impedance. **(A)** Data from IODP site U1505; **(B)** Data from IODP site U1501; **(C)** Data from ODP site 1148.

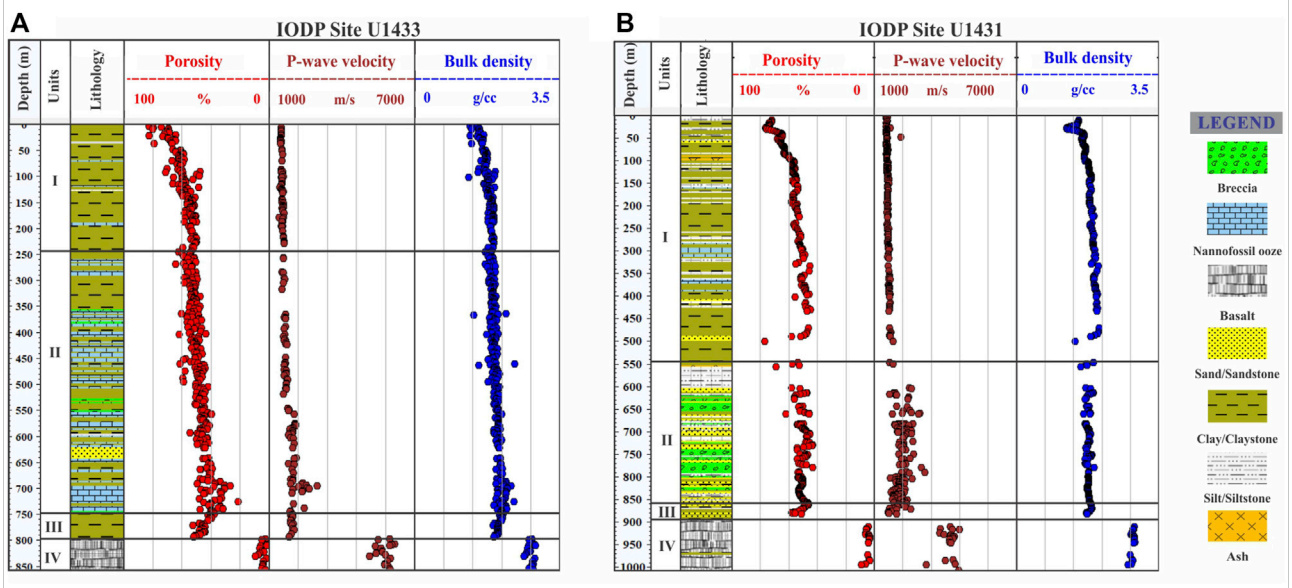

FIGURE 5
Core data results of the studied sites U1433 in the (SWSB) and U1431 in the (ESB), with measurements of moisture, density (MAD) and, P-wave velocity(PWC). **(A)** Data from IODP site U1433; **(B)** Data from IODP site U1431.

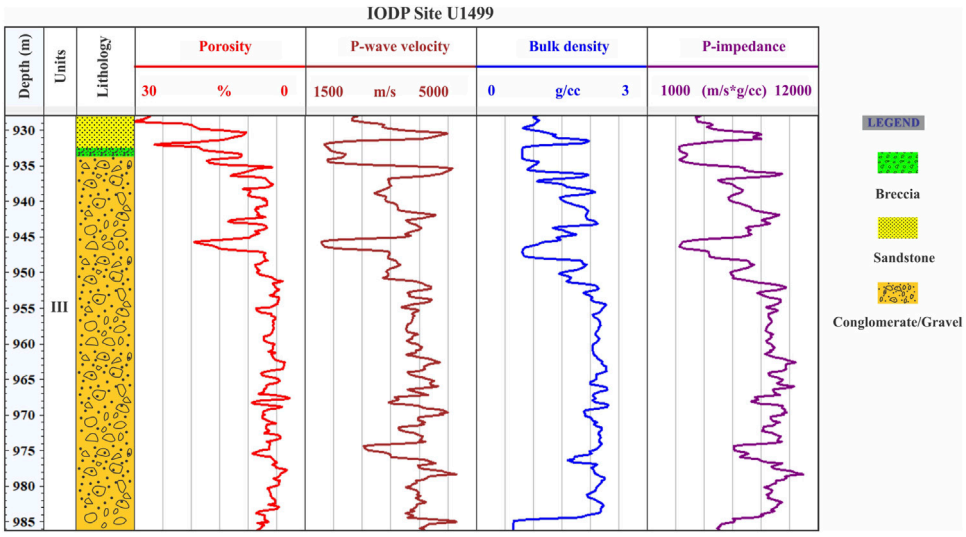

FIGURE 6
Logging curves of the pre-Oligocene interval of IODP Site U1499.

from 1.5 to 2.6 g/cc, and P-impedance from 3190 to 10600 m/s*g/cc while the porosity displays very low values from 29% to 3% (Figures 4B, 6). This variation indicates that the sandstone is quite different from Unit II to Unit III in terms of the physical properties (color, degree of lithification, and composition of clastic components, as shown in (Figure 3B). Therefore, we believethat Unit III was established not far from e littoral-terrestrial environment with an important erosional hiatus that formed in the late Mesozoic or possibly the beginning of the early Cenozoic period. By contrast, unit III at IODP Sites U1431 and U1433 represents the claystone layer recovered directly

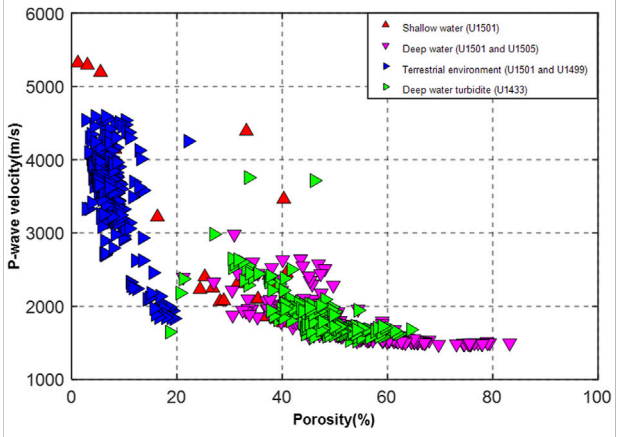

FIGURE 7
Cross plot of P-wave velocity versus porosity for IODP core data of sites U1501, U1505C, U1499, and U1433. Data points are color-coded by different depositional environments.

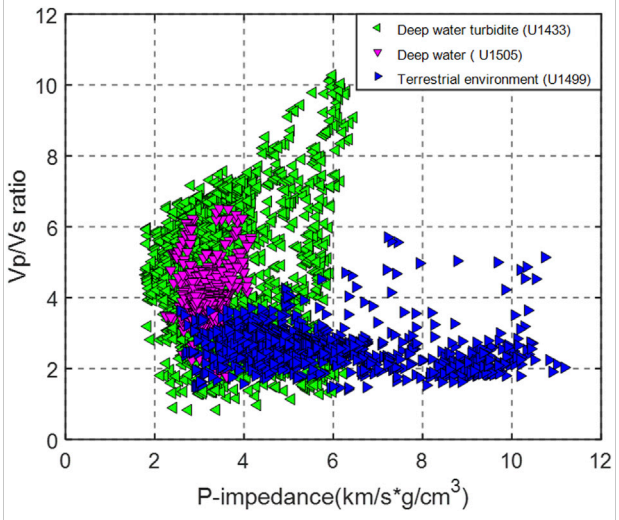

FIGURE 8
Cross plot of P-impedance versus Vp/Vs ratio for IODP logging data of sites U1505C, U1499, and U1433. Data points are color-coded by different depositional environments.

over the igneous basement. The rock physical characteristics exhibit a trend of decreasing density, from2.13 to 1.86 g/cc and P-wave velocity, from 2100 to 1800 m/s. While the porosity increases to 50%, mainly due to the substantial increase in clay content, which indicatesthat the site is located much closer to continental sediment sources (Figures 5A,B).

The lowermost lithologic Unit IV consists primarily of massive basalt lava flows that display a significant difference in the physical properties of the rocks. It is supported by an increase in both P-wave velocity and density, ranging from 3000 to 6300 m/s and from 2.6 to 2.9 g/cc, respectively, while the porosity is extremely low ranging from 1% to 14% (Figures 5A,B). Furthermore, the presence of a thin layer of clay within the basalt layer at both Sites U1431 and U1433 resulted in changes in physical properties, i.e., decreased velocity and bulk density and increased porosity values. This can be representing non-depositional hiatus between two basaltic flows.

Comparison of depositional environments at different sites on elastic characteristics

Figure 7 illustrates the influences of different depositional environments on the Vp-porosity relationship based on the IODP core data analysis. It is evident that different depositional environments exhibit distinct rock physics characteristics. In general, deep-water turbidite sediments show high porosity and low-velocity signatures. Most of the sediments fall along with the typical suspension trend (Han and Batzle, 2004), where the velocity is almost constantas porosity is smaller than critical porosity (the transition porosity from deposition status to diagenesis). It is also interesting to note that the critical porosity for deep-water turbidite sediments is around 40%, representing a typical value for clastic sediments, whereas the critical porosity for deep-water sediments is around 50%, representing a typical value for calcareous-rich sediment and ooze (Keys and Xu, 2002). Therefore, the Vp-porosity cross-plot as well as the characteristics of critical porosity can provide a clue for the lithofacies of different depositional environments. After crossing the critical porosity, the deep-water turbidite and sediments start to slightly increase as porosity decreases, suggesting the loosely compacted status and early diagenesis. It is necessary to point out that some high-velocity zone in the deep-water turbidite depositional environment corresponds to some carbonate layers which have gone through compaction and diagenesis (Li et al., 2015a).

Nevertheless, the shallow water and terrestrial environment overall show low porosity and high-velocity signatures. In particular, the steep velocity-porosity trend for the terrestrial environment suggests that those rocks are strongly affected by post-depositional diagenesis. For example, the clastic facies occurring in Unit II at the U1501 site contain coarse sand intervals, which indicates a terrigenous origin. In addition, the lowermost section (Unit III) from IODP sites U1499 and U1501 has coarse sand intervals that reach pebble-sized clasts, where the extensive diagenetic alteration makes those rocks exhibit higher velocities and lower porosity characteristics.

P-impedance and Vp/Vs ratio are two critical elastic parameters controlling seismic responses. Figure 8 shows the

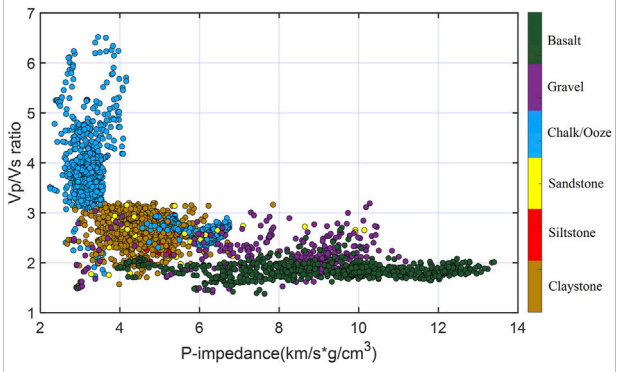

FIGURE 9
Cross plot of P-impedance versus Vp/Vs ratio based on the IODP logging data. Data points are color-coded by different lithofacies including- basalt, gravel, chalk/ooze, sandstone, siltstone, and claystone from different IODP Sites U1499,U1502, and U1505.

cross plot of the P-impedance versus Vp/Vs ratio corresponding to three different depositional environments. Generally, terrestrial environments have a higher P-impedance than deep-water and deep-water turbidite environments. The distinct elastic features mainly come from the different mineralogical content and porosity, which are also associated with the diagenetic features. The Vp/Vs ratio of sediments within the depositional environment of deep-water turbidite is very high. The chaotic and catastrophic depositional environment also makes the P-impedance (2–6 km/s *g/cc) and Vp/Vs ratio vary significantly in a wide range between 1.5 and 10, also reflecting the occurrence of complex lithofacies. The decreasing trend of P-impedance and Vp/Vs ratio within the depositional environment of deep-water turbidite is due to the increase of organic matter because the water depth in this stratum was deeper and thus more favorable for the accumulation of organic matter. It is also interesting to note that the Vp/Vs ratio of calcareous-rich sediment and ooze in the deep-water depositional environment also spans a relatively wide range from 2 to 6, whereas the P-impedance stays at a narrow range.

The influences of lithofacies and compaction on the elastic properties

The lithofacies of sediment sequences have a significant effect on the interrelationships of physical properties. Figure 9 shows the cross plot of the P-impedance and Vp/Vs ratio corresponding to the different lithofacies from the logging data of IODP Sites U1499, U1502, and U1505. Based on the IODP logging data analysis, the SCS can be subdivided into four types of lithofacies namely, 1) calcareous-rich sediment and ooze, 2) argillaceous clay, silt, and sand, 3) coarse sand intervals with up to pebble-sized clasts, 4) volcanic ash interlayer. The different lithofacies exhibit distinct rock physics characteristics.

As illustrated in Figure 9, for the nannofossil ooze/chalk lithofacies, which are exclusively developed in a marine water environment of the study area, the Vp/Vs ratio is significantly high and the P-impedance shows a typical lower value. The abundance of nannofossil ooze within these lithofacies indicated the existence of open ocean water with higher carbonate productivity and less terrestrial input. However, a few data points still exhibit high-impedance characteristics. Presumably, the heterogeneities prevailing in the thin layers with low porosity and high carbonate content are responsible for those outliers, which may be causedby variations in the environment of deposition or diagenesis (e.g., enhanced cementation).

Conversely, the lithofacies of coarse sand intervals show relatively high P-impedance and lower Vp/Vs ratio (Figure 9). Such types of lithofacies is exclusively developed in the terrestrial environment of the study area at IODP Sites U1499 of possible Eocene age. It is featured by sub-angular to angular pebbles and cobbles embedded in the rock body and represents sandstones of different sizes and textures. Finally, the lithofacies of the basaltic layer have high P-impedance ranging from 4 to 14 km/s *g/cc (mainly from IODP site of U1502). It is necessary to point out that the wide range of P-impedance is mainly because the basaltic layers are divided into two distinct zones: the upper brecciated zone shows low P-wave impedance values, while the lower massive basalt lava flows zone is characterized by a gradual increase of P-wave impedance (Planke et al., 1999). In contrast, the Vp/Vs ratio (<2) is confined in a narrow range (Figure 9).

Figure 10 illustrates the influences of physical compaction on the elastic characteristics of P-impedance and Vp/Vs ratio, which are color-coded by depth. It is apparent that physical compaction is also the primary factor controlling the P-impedance and Vp/Vs ratio, the two most important elastic parameters for quantitative seismic interpretation. As the depth increases, except for the igneous rocks, the Vp/Vs ratio gradually decreases and P-impedance gradually increases. This is of no surprise, as shear wave velocity is extremely sensitive to the consolidation degree of marine sediments, and hence the Vp/Vs ratio can decrease from 6 for the poorly consolidated sediments to 1.6 for the siltstone with considerable physical compaction. Note that the quite large range of Vp/Vs ratio for chalk/ooze (3–6) is mainly due to the compaction trend. The calcite content might also slightly contribute to the scattering of the Vp/Vs ratio in such a big range. In addition, the logging measurement of shear wave velocity in the very shallow depth is still challenging, which might also cause uncertainty and scatter in the data.

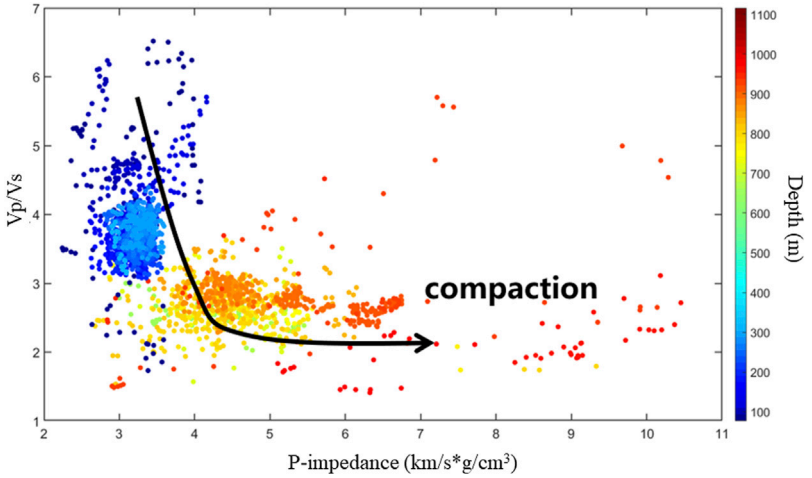

FIGURE 10
Influences of compaction on the elastic characteristics of P-impedance and Vp/Vs ratio. The data points are color coded by depth.

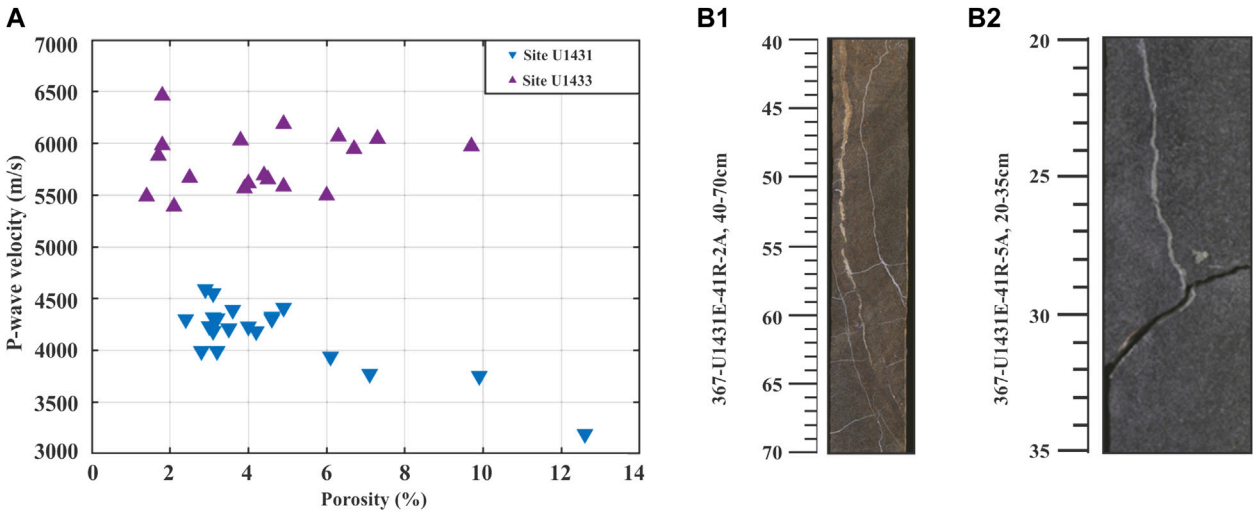

FIGURE 11
(A) Cross plots of P-wave velocity against porosity for basalt data of Sites U1431E and U1433B; **(B1)** Core photo showing the fracture in U1431E-41R-2A; **(B2)** Core photo showing the fracture in U1431E-41R-5A.

Effect of tectonic activity

The data from Sites U1431 and U1433 illustrate the effects of tectonic activity on the physical properties. In 2014, Expedition 349 Scientists found notable changes in the sedimentary facies between the U1431 and U1433 sites and hence a change in physical properties (Li et al., 2015a). It was evident that there were well-defined differences across the fossil ridge as well as the Zhongnan Fault/Ridge between the Southwest and East Sub-basins. This suggests that such structures served as significant sediment barriers, and there was long-term tectonic activity adjacent to this fault.

The main difference between Sites U1431 from the Northern East sub-basin and U1433 from the Southwest Sub-basin is the presence of massive carbonate deposition at Site U1433 from the Lower Pleistocene to the upper Miocene (Figure 2). This difference can be explained by the fact that the Southwest Sub-basin is nearby to the southern blocks that were capped with carbonates such as Reed Bank, Palawan, or Dangerous Grounds (Yao et al.,

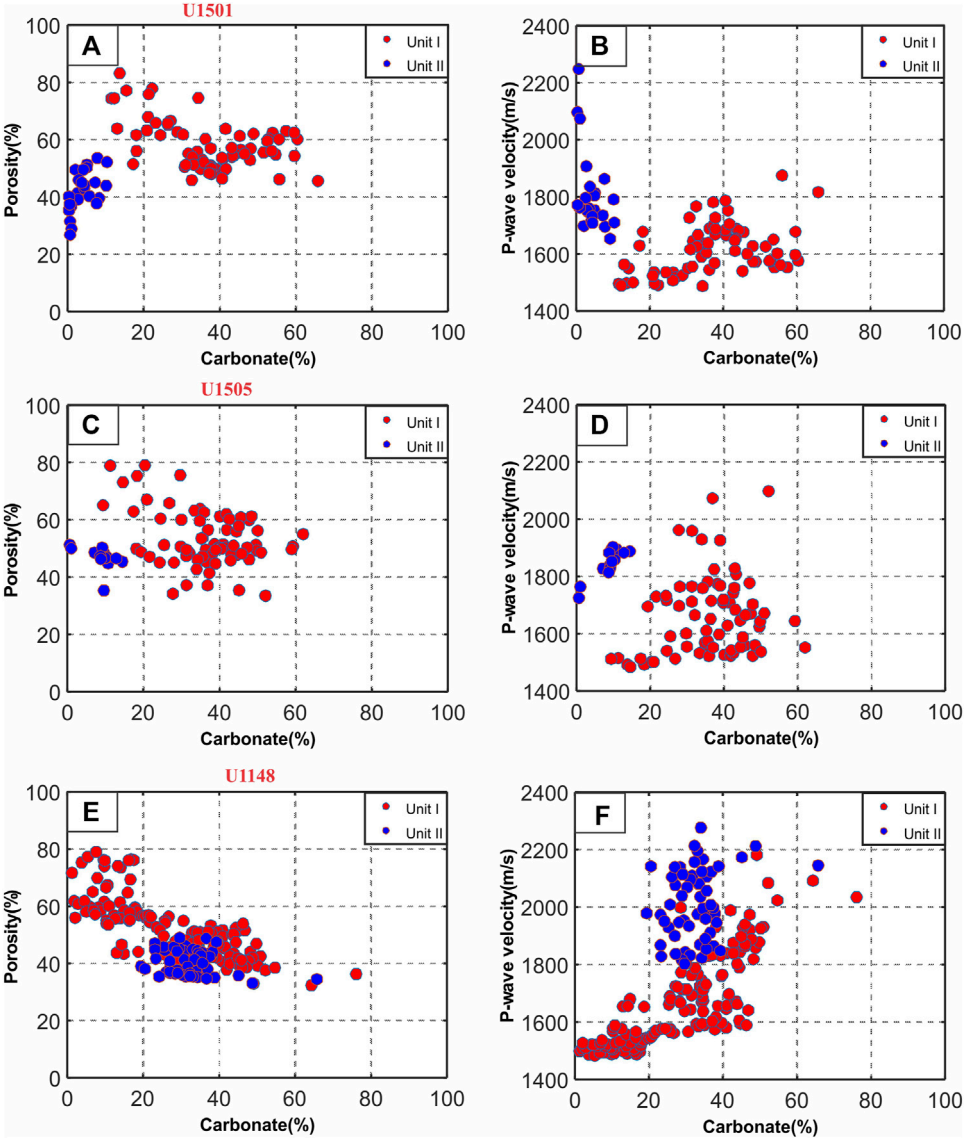

FIGURE 12
Porosity and P-wave velocity versus carbonate based on the ODP/IODP sites; **(A,B)** IODP U1501; **(C,D)** IODP U1505; **(E,F)** ODP site U1148. Data points are color-coded by different depositional units.

2012; Ding et al., 2013), and were carried into the central basin by turbidity currents (Li et al., 2015b). Conversely, the Northeast Sub-basin gained sediments with slightly less production of Miocene carbonate, mostly from the north. As a result, the upper Miocene sequence in the Southwest Sub-basin, which is dominated by deep water carbonate turbidite deposition, displays increasing trends of density and P-wave velocity while the porosity exhibits a decreasing trend (Figure 5).

In addition, as indicated in Figure 11A, the limited velocity measurement of basaltic core samples from Site U1431E show significant differences in P-wave velocity. This is mainly attributed to the higher frequency of fractures occuring at site U1431 compared to Site U1433, reflec a higher degree of alteration of the basalt. The comparatively reduced P-wave velocity approximated from the basaltic layers at Site U1431E could be related to the increased presence of cracks (Figures 11b1,b2) (Walsh, 1965; Toksöz et al., 1976), where the most active faulting currently occur much closer to site U1431 in the East Sub-basin, due to active subduction of the southern part of the Manila Trench, as well as the collision of the Luzon arc with the Northeast Palawan (Li et al., 2015b).

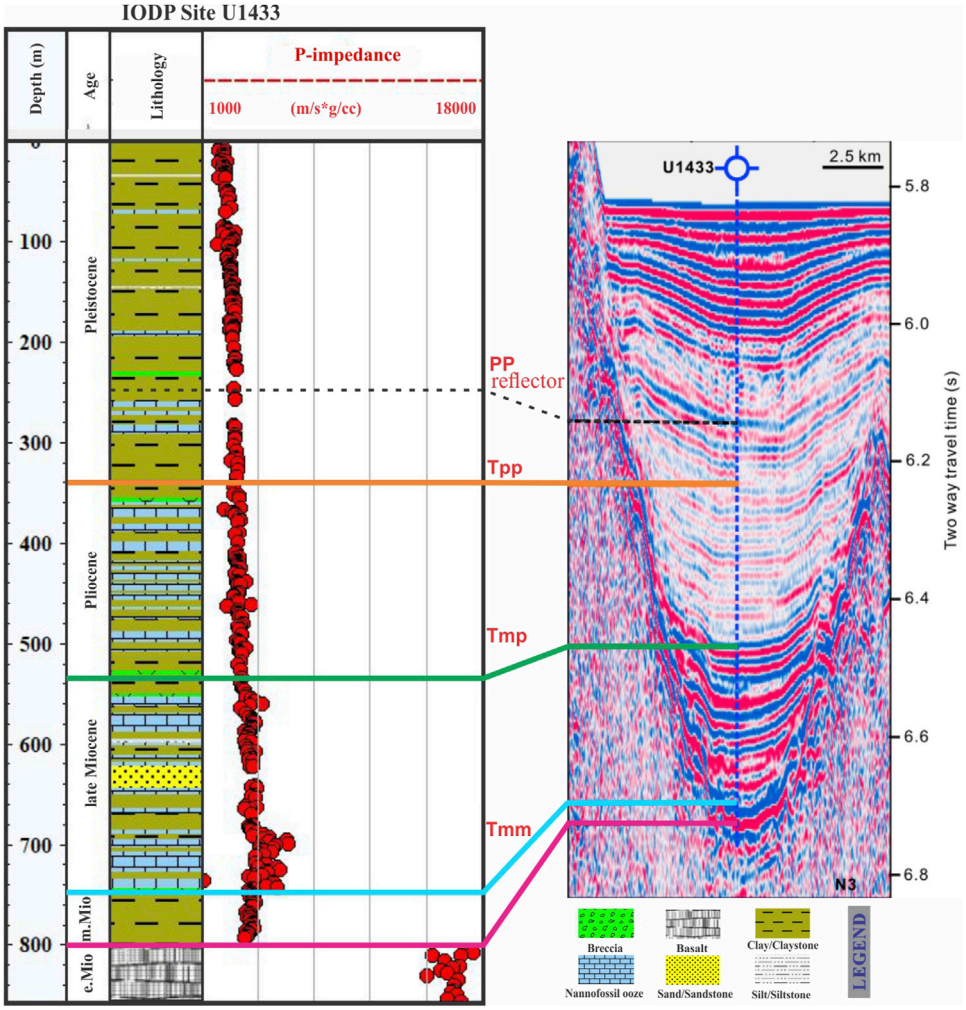

FIGURE 13
Seismic horizons at IODP Site U1433 in the Southwest sub-basin. Modified after (Li et al., 2015a).

Discussion

The effect of carbonate content on the rock physics characteristics

We can compare the relative effects of carbonate contents on rock physical properties by examining the data from Sites U1148, U1501, and U1505 at SCS. The CaCO3 contents of the study area samples varied between 0 and 80 wt% (Figures 12A–F). The low range of carbonate content comprised samples of terrigenous sediments, whereas the high carbonate samples mainly consisted of nannofossil ooze.

Figure 12 shows the cross plot of porosity and P-wave velocity versus carbonate content corresponding to different depositional units. Unit I is dominated by calcareous nannofossils and is distinguished by significantly higher carbonate content (an average of 47 wt%). This indicates a much more stable environment with a low supply of terrigenous material, which may be related to rising sea levels during this interval. The porosity overall decreases with the increase of carbonate content. This is mainly because the carbonate content increases with the increase of depth due to the enhanced carbonate productivity, and hence the porosity gradually increases with the mitigated compaction effects. It is also interesting to notice that different sites have different carbonate contents, which reflect decreasing carbonate productivity as well as increasing clastic input from Site U1501 to Site U1148. Nevertheless, the relationship of P-wave velocity-carbonate content becomes complicated. At Site U1501, the velocity is almost insensitive to the variation of carbonate content, since the porosity is over critical

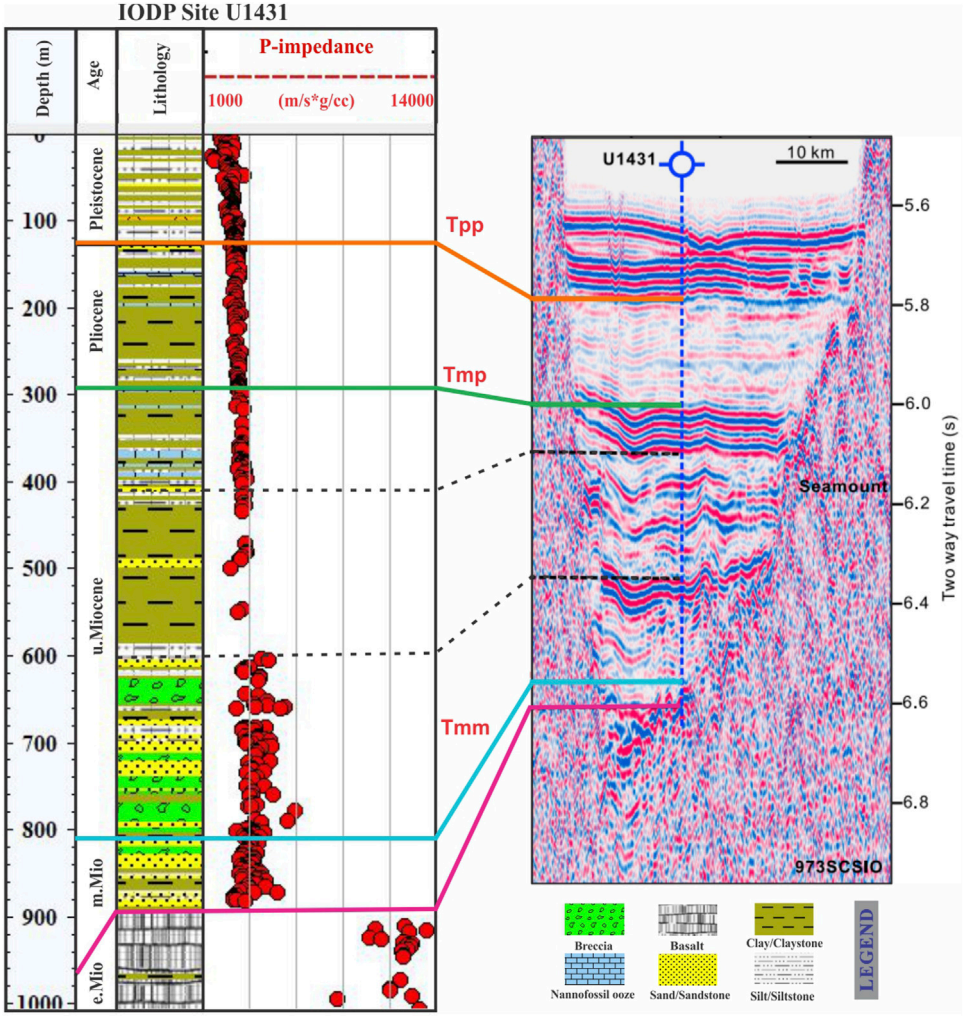

FIGURE 14
Seismic horizons at IODP Site U1431 in the East sub basin. Modified after (Li et al., 2015a).

porosity (~50%) and the marine sediments are in the suspension status. At Site U1148, the velocity exhibits an increasing trend with the increase of carbonate content, which is mainly because the porosity sharply decreases with increased carbonate content.

Unit II has low carbonate contents compared to Unit I indicating a high proportion of aquatic organic matter, but overall contains 8–10 wt% carbonate content at both IODP Sites U1501 and U1505. This is also linked to the change in depositional environment from shallow to deep water as the rate of clastic sedimentation increases, resulting in the accumulation of more detrital minerals. However, even within Unit II at IODP Site U1501, there are still some data points showing an increasing trend of porosity and carbonate content (Figure 12A), which are probably caused by the overall fining of clastic material indicating deepening basin conditions.

In contrast, Unit II at ODP Site U1148 shows a distinct increase in carbonate content compared to other sites ranging between 20–40 wt% and marked by a sharp increase in P-wave velocity, and a decrease in porosity (Figures 12E,F), reflecting a high biogenic silica accumulation during this unit.

Implications for seismic stratigraphy interpretation

Investigating the physical characteristics of rocks lay the groundwork for future seismic interpretation. The changes in

sedimentary facies between Sites U1431 and U1433 were revealed by changes in the seismic reflection and thus in rock physical properties. In the Southwest Sub-basin, the upper parts of the Pleistocene sequence are mainly composed of clay and nannofossil oozes by turbidite deposition. Although the P-impedance is very low, there exists significant impedance contrasts. Therefore, as shown in Figure 13, there arestrong seismic reflection. Nevertheless, the lower parts of the Pleistocene sequence are composed of mostly clays interbedded with carbonates, exhibiting uniform impedance variation and weaker seismic reflections (Figure 13).

The IODP cores show that the Pliocene sequences in the East Sub-basin consist primarily of clays whereas in the Southwest Sub-basin consist primarily of interbedded clays and carbonates; As shown in Figures 12, 13, they generally have very weak P-impedance contrast. As a consequence, Pliocene sequences are characterized by weaker seismic reflection at both Sites U1431 and U1433 in the East and Southwest Sub-basin, respectively.

In the East Sub-basin, the alteration between clay, silt, and carbonate in the upper part of the late Miocene sequence, and sand interbedded with volcanoclastic breccia in the lower part of it, characterized by a decrease in porosity and increases in density, P-wave velocity, and P-impedance. These observations explain the strong seismic reflection interface of strata in the upper and lower parts of the late Miocene sequence at IODP Site U1431 (Figure 14). Nevertheless, the middle part of the late Miocene sequences mainly composed of clay corresponds to weak P-impedance contrast, yielding a weaker seismic reflection interface (Figure 14).

In the Southwest Sub-basin, the lithologic interface between clays and massive carbonate in the late Miocene sequence show much higher velocity and P-impedance contrast. This explains the strong seismic reflection of strata in the late Miocene sequence at IODP Site U1433.

Conclusion

This study focuses on the analysis of the elastic properties of marine sediments in the SCS and their influencing factors based on the ODP/IODP sites. The main conclusions are given as follows:

1) The different depositional environments exhibit distinct rock physics characteristics. The sediments deposited in the shallow water and terrestrial environment exhibit higher velocities in comparison with the deep water and deep-water turbidite sediments
2) Across the boundary between the Oligocene-Miocene age, there are sharp decreases in velocities and densities, and an increase in porosity, indicating non-depositional hiatus formed in the sedimentary record at this boundary. This is also associated with a decrease in carbonate content from 65 to 10 wt%.
3) The lithofacies and compaction effects are mainly responsible for the variation of P-impedance and Vp/Vs ratio. With the enhanced compaction effects, the P-impedance exhibits an increasing trend while Vp/Vs ratio significantly decreases from 6 to less than 2.
4) The basalt samples at IODP Site U1433 having a P-wave velocity of 5500–6500 m/s differ significantly from basalt samples at IODP Site U1431 having a lower velocity of 3000–4500 m/s, which might be caused by more fractures occurred at Site U1431, suggesting the distinct tectonic activities along Fossils Spreading Ridge and Zhongnan Ridge/Faults.

Data availability statement

Publicly available datasets were analyzed in this study. This data can be found here: All the data analyzed in this study can be found at https://www.iodp.org/resources/access-data-and-samples.

Author contributions

All authors listed have made a substantial, direct, and intellectual contribution to the work and approved it for publication.

Funding

This work was supported by the National Key R&D Program of China (2018YFC0310105), Shanghai Rising-Star Program (21QA1409200), and Fundamental Research Funds for the Central Universities.

Conflict of interest

The authors declare that the research was conducted in the absence of any commercial or financial relationships that could be construed as a potential conflict of interest.

Publisher's note

References

Ayoub, V., Delenne, C., Chini, M., Finaud-Guyot, P., Mason, D., Matgen, P., et al. (2022). A porosity-based flood inundation modelling approach for enabling faster large scale simulations. *Adv. Water Resour.* 162, 104141. doi:10.1016/j.advwatres.2022.104141

Ba, J., Xu, W., Fu, L. Y., Carcione, J. M., and Zhang, L. (2017). Rock anelasticity due to patchy saturation and fabric heterogeneity: A double double-porosity model of wave propagation. *J. Geophys. Res. Solid Earth* 122 (3), 1949–1976. doi:10.1002/2016jb013882

Bassinot, F., Marsters, J. C., Mayer, L. A., and Wilkens, R. H. (1993). *Variations of porosity in calcareous sediments from the ontong java plateau*.Texas, TX, USA: Ocean Drilling Program College Station TX

Breitzke, M. (2000). Acoustic and elastic characterization of marine sediments by analysis, modeling, and inversion of ultrasonic P wave transmission seismograms. *J. Geophys. Res.* 105 (B9), 21411–21430. doi:10.1029/2000jb900153

Cai, W., Dou, L., Gong, S., Li, Z., and Yuan, S. (2015). Quantitative analysis of seismic velocity tomography in rock burst hazard assessment. *Nat. Hazards (Dordr).* 75 (3), 2453–2465. doi:10.1007/s11069-014-1443-6

Christeson, G. L., Gulick, S. P., Morgan, J. V., Gebhardt, C., Kring, D. A., Le Ber, E., et al. (2018). Extraordinary rocks from the peak ring of the chicxulub impact crater: P-Wave velocity, density, and porosity measurements from IODP/ICDP expedition 364. *Earth Planet. Sci. Lett.* 495, 1–11. doi:10.1016/j.epsl.2018.05.013

Courville, Z., Albert, M., Fahnestock, M., Cathles IV, L., and Shuman, C. (2007). Impacts of an accumulation hiatus on the physical properties of firn at a low-accumulation polar site. *J. Geophys. Res.* 112 (F2), F02030. doi:10.1029/2005jf000429

David, C., Menéndez, B., and Darot, M. (1999). Influence of stress-induced and thermal cracking on physical properties and microstructure of La Peyratte granite. *Int. J. Rock Mech. Min. Sci.* 36 (4), 433–448. doi:10.1016/s0148-9062(99)00010-8

Ding, W., Franke, D., Li, J., and Steuer, S. (2013). Seismic stratigraphy and tectonic structure from a composite multi-channel seismic profile across the entire Dangerous Grounds, South China Sea. *Tectonophysics* 582, 162–176. doi:10.1016/j.tecto.2012.09.026

Eberli, G. P., Baechle, G. T., Anselmetti, F. S., and Incze, M. L. (2003). Factors controlling elastic properties in carbonate sediments and rocks. *Lead. Edge* 22 (7), 654–660. doi:10.1190/1.1599691

Fabricius, I. L. (2014). Burial stress and elastic strain of carbonate rocks. *Geophys. Prospect.* 62 (6), 1327–1336. doi:10.1111/1365-2478.12184

Fabricius, I. L. (2007). Chalk: Composition, diagenesis and physical properties. *bgsd.* 55, 97–128. doi:10.37570/bgsd-2007-55-08

Franke, D., Barckhausen, U., Baristeas, N., Engels, M., Ladage, S., Lutz, R., et al. (2011). The continent-ocean transition at the southeastern margin of the South China Sea. *Mar. petroleum Geol.* 28 (6), 1187–1204. doi:10.1016/j.marpetgeo.2011.01.004

Gatter, R., Clare, M., Kuhlmann, J., and Huhn, K. (2021). Characterisation of weak layers, physical controls on their global distribution and their role in submarine landslide formation. *Earth-Science Rev.* 223, 103845. doi:10.1016/j.earscirev.2021.103845

Graw, J., Wood, W., and Phrampus, B. (2020). Predicting global marine sediment density using the random forest regressor machine learning algorithm. *J. Geophys. Res. Solid Earth* 126, e2020JB020135. doi:10.1029/2020jb020135

Hamilton, E. L., Bachman, R. T., Berger, W. H., Johnson, T. C., and Mayer, L. A. (1982). Acoustic and related properties of calcareous deep-sea sediments. *J. Sediment. Res.* 52 (3), 733–753.

Hamilton, E. L. (1972). Compressional-wave attenuation in marine sediments. *Geophysics* 37 (4), 620–646. doi:10.1190/1.1440287

Hamilton, E. L. (1980). Geoacoustic modeling of the sea floor. *J. Acoust. Soc. Am.* 68 (5), 1313–1340. doi:10.1121/1.385100

Hamilton, E. L. (1974). Prediction of deep-sea sediment properties: State-of-the-art. *Deep-Sea Sediments*, 1–43. doi:10.1007/978-1-4684-2754-7_1

Hamilton, E. L. (1976). Variations of density and porosity with depth in deep-sea sediments. *J. Sediment. Res.* 46 (2), 280–300.

Han, D.-h., and Batzle, M. L. (2004). Gassmann's equation and fluid-saturation effects on seismic velocities. *Geophysics* 69 (2), 398–405. doi:10.1190/1.1707059

Hou, Z., Chen, Z., Wang, J., Zheng, X., Yan, W., Tian, Y., et al. (2018). Acoustic impedance properties of seafloor sediments off the coast of Southeastern Hainan, South China Sea. *J. Asian Earth Sci.* 154, 1–7. doi:10.1016/j.jseaes.2017.12.003

Hughes, T. J., Henstock, T. J., Pilgrim, J. A., Dix, J. K., Gernon, T. M., and Thompson, C. E. (2015). Effect of sediment properties on the thermal performance of submarine HV cables. *IEEE Trans. Power Deliv.* 30 (6), 2443–2450. doi:10.1109/tpwrd.2015.2398351

Hutchison, C. S., and Vijayan, V. (2010). What are the Spratly islands? *J. Asian Earth Sci.* 39 (5), 371–385. doi:10.1016/j.jseaes.2010.04.013

Jian, Z., Jin, H., Kaminski, M. A., Ferreira, F., Li, B., and Yu, P.-S. (2019). Discovery of the marine Eocene in the northern South China sea. *Natl. Sci. Rev.* 6 (5), 881–885. doi:10.1093/nsr/nwz084

Kenter, J., Anselmetti, F., Kramer, P., Westphal, H., and Vandamme, M. (2002). Acoustic properties of" young" carbonate rocks, ODP leg 166 and boreholes Clino and Unda, weWesternreat Bahama Bank. *J. Sediment. Res.* 72 (1), 129–137. doi:10.1306/041101720129

Keys, R. G., and Xu, S. (2002). An approximation for the Xu-White velocity model. *Geophysics* 67 (5), 1406–1414. doi:10.1190/1.1512786

Kim, G.-Y., and Kim, D.-C. (2005). Sediment physical and acoustic properties at ODP sites 1150 and 1151, Japan Trench. *Mar. Georesources Geotechnol.* 23 (1-2), 1–11. doi:10.1080/10641190590944908

Larsen, H. C., Jian, Z., Alvarez Zarikian, C. A., Sun, Z., Stock, J. M., Klaus, A., et al. (2018). *Site U1501*. U S A: IODP. doi:10.14379/iodp.proc.367368.105.2018

Lee, E. Y., Tejada, M. L. G., Song, I., Chun, S. S., Gier, S., Riquier, L., et al. (2021). Petrophysical property modifications by alteration in a volcanic sequence at IODP Site U1513, Naturaliste Plateau. *JGR. Solid Earth* 126 (10), e2020JB021061. doi:10.1029/2020jb021061

Li, A. C., Huang, J., Jiang, H. Y., and Wan, S. M. (2011). Sedimentary evolution in the northern slope of the South China Sea since the Oligocene and its response to tectonics. *Chin. J. Geophys.* 54 (6), 1084–1096. doi:10.1002/cjg2.1686

Li, C.-F., Li, J., Ding, W., Franke, D., Yao, Y., Shi, H., et al. (2015a). Seismic stratigraphy of the central South China Sea basin and implications for neotectonics. *J. Geophys. Res. Solid Earth* 120 (3), 1377–1399. doi:10.1002/2014jb011686

Li, C.-F., Lin, J., Kulhanek, D., Williams, T., Bao, R., Briais, A., et al. (2015b). *Expedition 349 summary*. U S A: IODP.

Li, C. F., Lin, J., Kulhanek, D. K., Williams, T., Bao, R., Briais, A., et al. (2014). Opening of the south China sea and its implications for southeast asian tectonics, climates, and deep mantle processes since the late mesozoic. *Integr. Ocean. Drill. Program Prelim. Rep.* 349, 1.

Lyu, C., Park, J., and Carlos Santamarina, J. (2021). Depth-dependent seabed properties: Geoacoustic assessment. *J. Geotech. Geoenviron. Eng.* 147 (1), 4020151. doi:10.1061/(asce)gt.1943-5606.0002426

Ma, R., Liu, C., Li, Q., and Jin, X. (2019). Calcareous nannofossil changes in response to the spreading of the South China Sea basin during Eocene-Oligocene. *J. Asian Earth Sci.* 184, 103963. doi:10.1016/j.jseaes.2019.103963

Martin, K. M., Wood, W. T., and Becker, J. J. (2015). A global prediction of seafloor sediment porosity using machine learning. *Geophys. Res. Lett.* 42 (24), 10,640–610,646. doi:10.1002/2015gl065279

Nobes, D., Mienert, J., and Dirksen, G. (1991). *Lithologc control of physical-property interrelationships*. Boulder, CO, USA: The Geological Society of America, 35.

Planke, S., Cerney, B., Bücker, C. J., and Nilsen, O. "Alteration effects on petrophysical properties of subaerial flood basalts: Site 990, Southeast Greenland margin," in *Proceedings of the ocean drilling Program scientific results* (Texas, TX, USA: Ocean Drilling Program College Station TX), 17–28.(Year)

Pola, A., Crosta, G., Fusi, N., Barberini, V., and Norini, G. (2012). Influence of alteration on physical properties of volcanic rocks. *Tectonophysics* 566, 67–86. doi:10.1016/j.tecto.2012.07.017

Richardson, M., Lavoie, D., and Briggs, K. (1997). Geoacoustic and physical properties of carbonate sediments of the Lower Florida Keys. *Geo-Marine Lett.* 17 (4), 316–324. doi:10.1007/s003670050043

Stewart, D., Studds, P., and Cousens, T. (2003). The factors controlling the engineering properties of bentonite-enhanced sand. *Appl. Clay Sci.* 23 (1-4), 97–110. doi:10.1016/s0169-1317(03)00092-9

Sun, Z., Jian, Z., Stock, J., Larsen, H., Klaus, A., and Alvarez Zarikian, C. (2018). The expedition 367/368 Scientists. 2018. South China sea rifted margin. *Proc. Int. Ocean Discov. Program* 367, 368.

Toksöz, M. N., Cheng, C., and Timur, A. (1976). Velocities of seismic waves in porous rocks. *Geophysics* 41 (4), 621–645. doi:10.1190/1.1440639

Urmos, J. (1994). *Diagenetic and physical properties of pelagic carbonate sediments: ODP leg 130, ontong java plateau*. Manoa, Hawai: University of Hawai'i at Manoa.

Van der Lingen, G., and Packham, G. (1975). Relationships between diagenesis and physical properties of biogenic sediments of the ontong-java plateau (sites 288 and 289, deep sea drilling project). *Init. Rep. DSDP* 30, 443–481.

Walsh, J. (1965). The effect of cracks on the compressibility of rock. *J. Geophys. Res.* 70 (2), 381–389. doi:10.1029/jz070i002p00381

Wang, Y., Han, D.-H., Zhao, L., Li, H., Long, T., and Hamutoko, J. (2021). Static and dynamic bulk moduli of deepwater reservoir sands: Influence of pressure and fluid saturation. *Lithosphere* 2021 (3). (Special). doi:10.2113/2022/4266697

Xie, Y., Wu, T., Sun, J., Zhang, H., Wang, J., Gao, J., et al. (2018). Sediment compaction and pore pressure prediction in deepwater basin of the South China Sea: Estimation from ODP and IODP drilling well data. *J. Ocean. Univ. China* 17 (1), 25–34. doi:10.1007/s11802-018-3449-2

Yan, Q., Shi, X., and Castillo, P. R. (2014). The late mesozoic–cenozoic tectonic evolution of the south China sea: A petrologic perspective. *J. Asian Earth Sci.* 85, 178–201. doi:10.1016/j.jseaes.2014.02.005

Yao, Y., Liu, H., Yang, C., Han, B., Tian, J., Yin, Z., et al. (2012). Characteristics and evolution of cenozoic sediments in the liyue basin, SE South China sea. *J. Asian Earth Sci.* 60, 114–129. doi:10.1016/j.jseaes.2012.08.003

Ymd, T. (1973). Factors controlling maximum and minimum densities of sands. *Eval. Relat. density its role geotechnical Proj. Involv. cohesionless soils* 523, 98.

Zhang, L., Ba, J., Carcione, J. M., and Fu, L.-y. (2020). Differential poroelasticity model for wave dissipation in self-similar rocks. *Int. J. Rock Mech. Min. Sci.* 128, 104281. doi:10.1016/j.ijrmms.2020.104281

Zhang, L., Ba, J., and Carcione, J. M. (2021). Wave propagation in infinituple-porosity media. *J. Geophys. Res. Solid Earth* 126 (4), e2020JB021266. doi:10.1029/2020jb021266

Zhao, L., Wang, Y., Liu, X., Zhang, J., Liu, Y., Qin, X., et al. (2020). Depositional impact on the elastic characteristics of the organic shale reservoir and its seismic application: A case study of the longmaxi-wufeng shale in the fuling gas field, sichuan basin. *Geophysics* 85 (2), B23–B33. doi:10.1190/geo2019-0326.1

Zhou, X., Lyu, X., Liu, C., Liu, Z., Li, Q., Jin, X., et al. (2019). Depositional mechanisms for upper Miocene sediments in the South China Sea central basin: Evidence from calcareous nannofossils. *Mar. Micropaleontol.* 151, 101768. doi:10.1016/j.marmicro.2019.101768